J. Non-Newtonian Fluid Mech. 165 (2010) 196–202

Contents lists available at ScienceDirect

Journal of Non-Newtonian Fluid Mechanics

journal homepage: www.elsevier.com/locate/jnnfm

Shear banding and interfacial instability in planar Poiseuille flow

Suzanne M. Fielding [a], Helen J. Wilson [b,*]

[a] Department of Physics, University of Durham, Science Laboratories, South Road, Durham DH1 3LE, United Kingdom
[b] Department of Mathematics, University College London, Gower Street, London WC1E 6BT, United Kingdom

ARTICLE INFO

Article history:
Received 2 September 2009
Received in revised form 1 December 2009
Accepted 3 December 2009

PACS:
47.50.+d
47.20.−k
36.20.−r

Keywords:
Shear banding
Interfacial instability
Poiseuille flow

ABSTRACT

Motivated by the need for a theoretical study in a planar geometry that can easily be implemented experimentally, we study the pressure driven Poiseuille flow of a shear banding fluid. After discussing the "basic states" predicted by a one-dimensional calculation that assumes a flat interface between the bands, we proceed to demonstrate such an interface to be unstable with respect to the growth of undulations along it. We give results for the growth rate and wavevector of the most unstable mode that grows initially, as well as for the ultimate flow patterns to which the instability leads. We discuss the relevance of our predictions to the present state of the experimental literature concerning interfacial instabilities of shear banded flows, in both conventional rheometers and microfluidic channels.

1. Introduction

Complex fluids have internal mesoscopic structure that is readily reorganised by an imposed shear flow. This reorganisation in turn feeds back on the flow field, resulting in strongly nonlinear constitutive properties. In some systems this nonlinearity is so pronounced that the underlying constitutive curve relating shear stress T_{xy} to shear rate $\dot{\gamma}$ in homogeneous flow is predicted to have a region of negative slope $dT_{xy}/d\dot{\gamma} < 0$ [1,2]. In this regime, an initially homogeneous flow is unstable to the formation of coexisting shear bands of differing local viscosities and internal structuring, with band normals in the flow-gradient direction y [3]. The signature of this transition in bulk rheometry is the presence of characteristic kinks, plateaus and non-monotonicities in the composite flow curve [4]. Explicit observation of the bands is made using local rheological techniques such as flow birefringence [5] and nuclear magnetic resonance [6,7], ultrasound [8,9], heterodyne dynamic light scattering [10,9] or particle image [11] velocimetry. Using these methods, the existence of shear banding has been firmly established in a wide range of complex fluids, including wormlike [4–6,12–19] and lamellar [20–25] surfactants; side-chain liquid crystalline polymers [26]; viral suspensions [27,28]; telechelic polymers [29]; soft glasses [30–32]; polymer solutions [33]; and colloidal suspensions [34].

Beyond the basic observation of shear banding, experiments with enhanced spatial and temporal resolution have more recently revealed the presence of complex spatio-temporal patterns and dynamics in many shear banded flows [8,24,25,33,35–49]. In many such cases, the bulk stress response of the system to a steady imposed shear rate (or vice versa) is intrinsically unsteady, showing either temporal oscillations or erratic fluctuations about the average (flow curve) value. Local rheological measurements reveal such signals commonly to be associated with a complicated behaviour of the interface between the bands [8,24,33,35,36,39,41–43,47–49]. The majority of these measurements have been in one spatial dimension (1D), normal to the interface between the bands. However 2D observations in Refs. [47,48] explicitly revealed the presence of undulations along the interface, in a boundary driven curved Couette flow, accompanied by Taylor-like vortices [49]. The undulations were shown to be either static or dynamic, according to the imposed flow parameters.

Theoretically, instability of an initially flat interface between shear bands was predicted in boundary driven planar Couette flow in Refs. [50–52]. In this work, separate 2D studies in the flow/flow-gradient (x–y) [50,51] and flow-gradient/vorticity (y–z) [52] planes revealed instability with respect to undulations along the interface with wavevector in the flow and vorticity directions respectively. In both cases the mechanism for instability was suggested to be a jump in normal stress across the interface [53].

* Corresponding author.
E-mail addresses: suzanne.fielding@durham.ac.uk (S.M. Fielding), helen.wilson@ucl.ac.uk (H.J. Wilson).

0377-0257/$ – see front matter © 2009 Elsevier B.V. All rights reserved.
doi:10.1016/j.jnnfm.2009.12.001

While these predictions provide a good starting point, there remains the possibility that the interfacial undulations observed in Refs. [47–49] originate instead in curvature driven effects such as a bulk viscoelastic instability of the Taylor Couette [54] type in the high shear band, as discussed in Ref. [49]. These were neglected in the planar calculations of Refs. [50–52] (Other possibilities, also neglected, include free surface instabilities at the open rheometer edges; and an erratic stick-slip motion at the solid walls of the flow cell. We shall not consider these further in what follows here either.)

In principle, therefore, either (or both) of (at least) two possible mechanisms could underlie the observed interfacial undulations: (i) a bulk viscoelastic Taylor Couette like instability of the strongly sheared band, or (ii) instability of the interface between the bands, driven by the normal stress jump across it. Of these, scenario (i) can only arise in a curved geometry. A possible experimental route to discriminating between these two scenarios is to perform rheology on the pure high shear branch, thereby eliminating the interface required for (ii). This is technically difficult, although the results of Ref. [55] suggest stability of the high shear phase alone. Another possible way to compare (i) and (ii) is to perform experimental studies in a planar flow geometry, thereby eliminating the curvature required for (i). However they are technically difficult to implement in a boundary driven setup.

There thus exists a clear need for theoretical predictions in a planar flow geometry that could easily be implemented experimentally. An obvious candidate comprises pressure driven flow in a rectilinear microchannel of rectangular cross-section with a high aspect ratio $L_z/L_y \gg 1$. Indeed, such experiments have recently been performed [56–58], as discussed in more detail below. With this motivation in mind, in this paper we study the planar Poiseuille flow of a shear banding fluid driven along the main flow direction x by a constant pressure drop $\partial_x P = -G$. For simplicity we assume the fluid to be sandwiched between stationary infinite parallel plates at $y = \{0, L_y\}$, neglecting the lateral walls in the z direction, and so taking the limit $L_z/L_y \to \infty$ at the outset. Our main contribution will be to show an interface between shear bands to be unstable in this pressure driven geometry, as it is in the boundary driven planar Couette flow studied previously [50–52]. We will furthermore give results for the growth rate and wavevector associated with the early stage kinetics of this instability, as well as the ultimate flow patterns to which it leads.

The paper is structured as follows. After introducing the rheological model and boundary conditions in Section 2, we calculate in Section 3 the one-dimensional (1D) shear banded states that are predicted when spatial variations are permitted only in the flow-gradient direction y, artificially assuming translational invariance in x and z, and accordingly assuming a flat interface between the bands. These form the "basic states" and initial conditions to be used in the stability calculations of the rest of the paper.

In Section 4 we study the linear stability of these 1D basic states with respect to small amplitude perturbations with wavevector $q_x\hat{\mathbf{x}}$ in the flow direction. As in the case of boundary driven flow studied previously, we find an undulatory instability of the interface between the bands [50–52]. Results are then presented for the ultimate nonlinear dynamical attractor in this x–y plane, from simulations that adopt periodic boundaries in x. This exhibits interfacial undulations of finite amplitude that convect along the flow direction at a constant speed. In Section 5 we turn instead to the flow-gradient/vorticity plane y–z, likewise demonstrating linear instability of the interface with respect to small amplitude perturbations with wavevector $q_z\hat{\mathbf{z}}$. We also give results for the ultimate nonlinear flow state, which in this plane is steady. Directions for future work, which will include full 3D calculations, are discussed in Section 6.

2. Model and geometry

The generalised Navier–Stokes equation for a viscoelastic material in a Newtonian solvent of viscosity η and density ρ is

$$\rho(\partial_t + \mathbf{v}\cdot\nabla)\mathbf{v} = \nabla\cdot(\mathbf{T} - P\mathbf{I}) = \nabla\cdot(\boldsymbol{\Sigma} + 2\eta\mathbf{D} - P\mathbf{I}), \tag{1}$$

where $\mathbf{v}(\mathbf{r}, t)$ is the velocity field and $\mathbf{D}$ is the symmetric part of the velocity gradient tensor, $(\nabla\mathbf{v})_{\alpha\beta} \equiv \partial_\alpha v_\beta$. Throughout we will assume zero Reynolds' number $\rho = 0$; and fluid incompressibility,

$$\nabla\cdot\mathbf{v} = 0. \tag{2}$$

The quantity $\boldsymbol{\Sigma}(\mathbf{r}, t)$ in Eq. (1) is the extra stress contributed to the total stress $\mathbf{T}(\mathbf{r}, t)$ by the viscoelastic component. We assume this to obey the diffusive Johnson–Segalman (DJS) model [59,60]

$$(\partial_t + \mathbf{v}\cdot\nabla)\boldsymbol{\Sigma} = a(\mathbf{D}\cdot\boldsymbol{\Sigma} + \boldsymbol{\Sigma}\cdot\mathbf{D}) + (\boldsymbol{\Sigma}\cdot\boldsymbol{\Omega} + \boldsymbol{\Omega}\cdot\boldsymbol{\Sigma}) + 2G_0\mathbf{D} - \frac{\boldsymbol{\Sigma}}{\tau} + \frac{\ell^2}{\tau}\nabla^2\boldsymbol{\Sigma}. \tag{3}$$

Here a is a slip parameter describing non-affinity of molecular deformation, i.e., the fractional stretch of the polymeric material with respect to that of the flow field. For $|a| < 1$ (slip) the intrinsic constitutive curve is capable of the non-monotonicity of Fig. 1, thereby admitting a shear banding instability. G_0 is a plateau modulus, τ is the viscoelastic relaxation time, and $\boldsymbol{\Omega}$ is the antisymmetric part of the velocity gradient tensor. The diffusive term $\nabla^2\boldsymbol{\Sigma}$ is needed to correctly capture the structure of the interface between the shear bands, with a slightly diffusive interfacial thickness $O(l)$, and to ensure unique selection of the shear stress at which banding occurs [61].

Within this model we study flow between infinite flat parallel plates at $y = \{0, L_y\}$. The fluid is driven in the positive x direction by a constant pressure gradient $\partial_x p = -G$, the plates being held stationary. Accordingly, we write Eq. (1) (at the zero Reynolds number of interest here) in the form

$$0 = \nabla\cdot(\boldsymbol{\Sigma} + 2\eta\mathbf{D} - \tilde{P}\mathbf{I}) + G\hat{\mathbf{x}}, \tag{4}$$

in which we have separated the main driving pressure gradient from the rest of the pressure field, $\tilde{P}$. Fluid incompressibility is enforcing by casting the fluid velocity in terms of streamfunctions; and $\tilde{P}$ is eliminated by taking the curl of Eq. (4). (The $q_x = 0$, $q_z = 0$ part of Eq. (4), containing G but not $\tilde{P}$, is dealt with

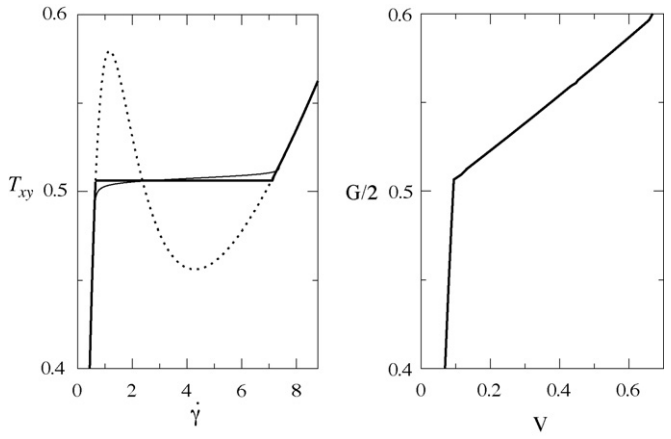

Fig. 1. *Left*: Dotted line: homogeneous constitutive curve for $a = 0.3$, $\eta = 0.05$. Thick solid line: composite flow curve for one-dimensional planar shear banded Couette flow (data already published in Ref. [50]). Selected stress $T_{sel} = 0.506$. Thin solid line: parametric plot of local shear stress $T_{xy}(y) = \Sigma_{xy}(y) + \eta\dot{\gamma}(y) = G((1/2) - y)$ against local shear rate $\dot{\gamma}(y)$ for one-dimensional planar shear banded Poiseuille flow with $l = 0.00125$, $G = 2.0$. *Right*: Halved pressure gradient versus total throughput for one-dimensional planar Poiseuille flow with $a = 0.3$, $\eta = 0.05$, $l = 0.0025$. This shows a kink at the onset of banding at $G/2 = T_{sel}$ as expected.

separately.) These two procedures are described in detail in the flow-gradient/vorticity plane in Section V of Ref. [52]; and in the flow/flow-gradient plane in Section II of Ref. [62].

At the plates we assume conditions of zero flux normal to the wall $\hat{\vec{n}} \cdot \nabla \Sigma_{\alpha\beta} = 0 \quad \forall \alpha, \beta$ for the viscoelastic stress (although other choices are possible [63,64]), with no slip and no permeation for the fluid velocity. Throughout we use units in which $G_0 = 1$, $\tau = 1$ and $L_y = 1$. Unless otherwise stated we use a (dimensionless) value $\eta = 0.05$, suggested by the experiments of Refs. [56]. We take $a = 0.3$, although our results are quite robust with respect to variations in this quantity. An order of magnitude estimate suggests $l = O(10^{-3})$ [65].

3. One-dimensional basic state

In this section we discuss the flow curves and shear banded states predicted by 1D calculations that allow spatial variations only in the flow-gradient direction y, assuming (often artificially) translational invariance in the flow direction x and vorticity direction z. As a warm-up discussion to the case of planar Poiseuille flow that forms the primary interest of this paper, we review first the more familiar case of planar Couette flow.

In steady 1D planar Couette flow, the shear stress T_{xy} is uniform across the flow cell. This follows trivially from solving Eq. (1) in this geometry. Within the (often artificial) assumption of a similarly homogeneous shear rate field, corresponding to a velocity field $\mathbf{v} = \dot{\gamma} y \hat{\vec{x}}$, the constitutive relation is then given by $T_{xy}(\dot{\gamma}) = \Sigma_{xy}(\dot{\gamma}) + \eta\dot{\gamma}$, where $\Sigma_{xy}(\dot{\gamma})$ follows as the xy component of the solution of Eq. (3) obtained by assuming stationarity in time and homogeneity in space. See the dotted line in Fig. 1(Left). For an applied shear rate in the region of negative slope $dT_{xy}/d\dot{\gamma} < 0$, homogeneous flow is predicted to be linearly unstable with respect to the formation of shear bands. The steady state composite flow curve is then shown by the thick solid line in the same figure. For shear stresses $T_{xy} < T_{\rm sel}$ (resp. $T_{xy} > T_{\rm sel}$), where the selected stress $T_{\rm sel} = 0.506$ for the particular choice of parameters in Fig. 1, the system shows homogeneous flow on the low shear (resp. high shear) branch of the constitutive curve. Applying a value of the shear rate $\bar{\dot{\gamma}}$ in the window between these branches, we obtain shear bands that coexist at the selected stress $T_{xy} = T_{\rm sel}$.

In steady 1D planar Poiseuille flow driven by a pressure drop $\partial_x P = -G$, Eq. (1) dictates the shear stress to be linear across the flow cell: $T_{xy} = -G(y - (1/2))$. Well away from any interfaces (the almost vertical regions in Fig. 2, Right) the value of the shear rate $\dot{\gamma}$ then follows as the lower (resp. upper) solution branch of the same relation $T_{xy}(\dot{\gamma}) = \Sigma_{xy}(\dot{\gamma}) + \eta\dot{\gamma}$ discussed above for planar Couette flow, in the regions where $|T_{xy}| < T_{\rm sel}$ (resp. $|T_{xy}| > T_{\rm sel}$). This leads to the steady flow states shown in Fig. 2, which are shear banded for all values of the applied pressure drop $G > 2T_{\rm sel}$ shown. In bulk rheology, the signature of the transition to shear banded flow is the pronounced kink seen in the composite flow curve of Fig. 1(Right).

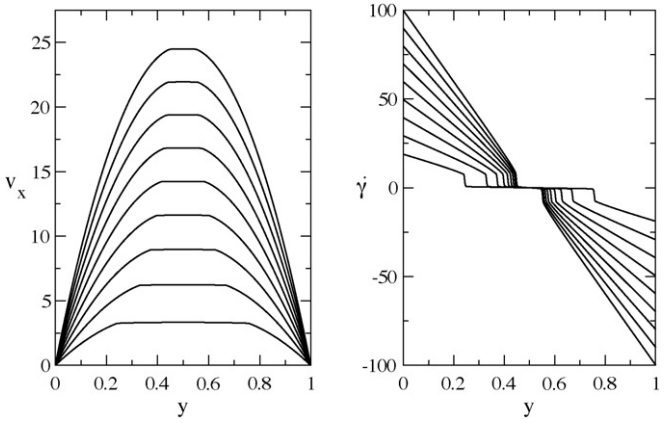

Fig. 2. *Left*: Velocity profiles in one-dimensional planar shear banded Poiseuille flow for $a = 0.3$, $\eta = 0.05$, $l = 0.0025$. Increased throughputs correspond to increased applied pressure gradients G = 2.0, 3.0, 4.0, 5.0, 6.0, 7.0, 8.0, 9.0, 10.0. *Right*: Corresponding shear rate profiles, which follow as the spatial derivative of the velocity profiles.

The 1D shear banded flows discussed in this section will form the basic states and initial conditions for the stability studies of the rest of the paper. In Section 4 we will consider 2D flow in the x–y plane, with periodic boundaries in the flow direction x, and assuming translational invariance in z. In Section 5 we will turn to 2D flow in the y–z plane, with periodic boundaries in the vorticity direction z, and assuming translational invariance in x.

4. Flow, flow-gradient plane

In this section we relax the assumption of translational invariance in the flow direction x and perform a two-dimensional study in the flow/flow-gradient (x–y) plane. As before we consider flow between closed walls at $y = \{0, L_y\}$, driven by a constant pressure drop $\partial_x p = -G$. The boundaries in x are taken to be periodic. For simplicity, translational invariance is still assumed in the vorticity direction z.

Our study comprises two parts. In Section 4.1 we study the linear stability of the 1D shear banded basic states of Fig. 2 with respect to perturbations that have infinitesimal amplitude and a wavevector $q_x\hat{\mathbf{x}}$ in the flow direction. We will show these basic states to be linearly unstable to such perturbations in most regimes. An initial condition comprising shear banded flow with a flat interface is thereby predicted to evolve towards a 2D state that has modulations along the interface, via the growth of these perturbations. In Section 4.2 we study the model's full nonlinear dynamics in this x–y plane, giving results for the ultimate 2D flow state that is attained once these modulations have grown to, and (as we shall demonstrate) saturated at, a finite amplitude.

Before presenting our results we discuss briefly our numerical method. In previous work the full nonlinear dynamics of the DJS model in boundary driven planar Couette flow with an average applied shear rate $\bar{\dot{\gamma}}$ were simulated in the flow/flow-gradient plane [66], assuming translational invariance in the vorticity direction. During the course of that study, the code was carefully checked against an earlier calculation of the linear stability of an interface between shear bands in planar Couette flow [50,51], providing a stringent check that the nonlinear code was working correctly. For the case of pressure driven planar Poiseuille flow of interest here, the equations to be solved are the same as in the earlier work, with the simple addition of the term $G\hat{\mathbf{x}}$ on the right hand side of Eq. (4). The numerical code can therefore be used precisely as in the earlier work, simply by (i) setting $\bar{\dot{\gamma}} = 0$ on the command line and (ii) adding an extra contribution $-G/\eta$ to the source term in the force balance equation (predivided by η for convenience) at zero wavevector (that is, to the right hand side of Eq. (18) in Ref. [52], where a full description of our numerical technique can be found).

4.1. Linear stability analysis

In each run of this modified code we start with an initial condition comprising a 1D banded state of Section 3, corresponding to shear banded flow with a flat interface between the bands. To this state we add 2D perturbations of tiny amplitude. By monitoring in this fully nonlinear code the growth of the Fourier components $\exp(iq_x x)\exp(\omega t)$ of the perturbation at the early times for which these perturbations are still tiny, we can extract the dispersion relation $\omega(q_x)$ that characterises the linear instability of the 1D

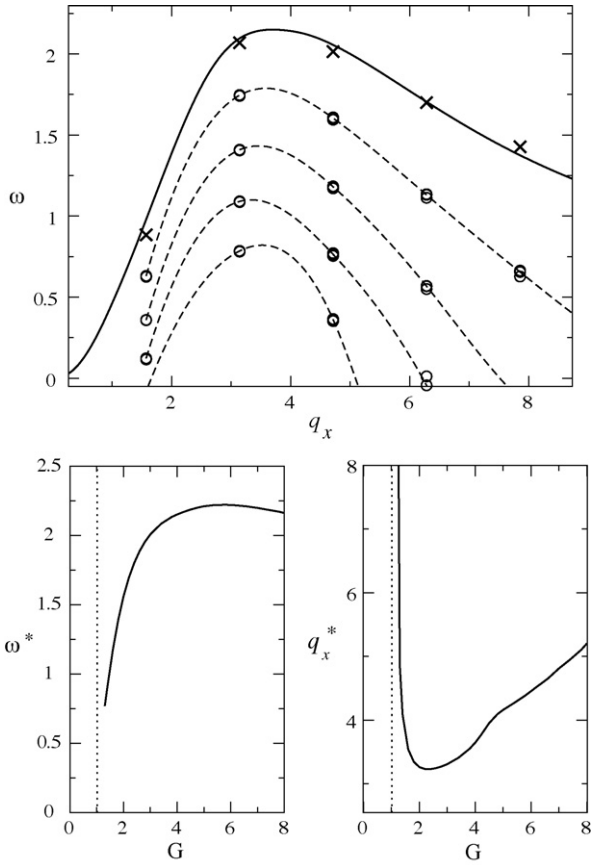

Fig. 3. *Top*: Dispersion relation of growth rate ω versus wavevector q_x during the initial stage of 2D instability, starting with a 1D shear banded planar Poiseuille basic state. In each case $a = 0.3$, $\eta = 0.05$, $G = 4.0$. Circles: extracted from early-time dynamics of the full nonlinear code. Groups of data upward correspond to l = 0.02, 0.015, 0.01, 0.005. Within each group, data are shown for $(Dt, N_x, N_y) = (0.000025, 200, 400)$, $(0.0000125, 200, 400)$, $(0.000025, 400, 800)$. These are mostly indistinguishable, demonstrating convergence with respect to grid and timestep. Dashed lines: cubic splines through the data for $(Dt, N_x, N_y) = (0.000025, 200, 400)$, as a guide to the eye. $L_x = 4.0$ in each case. Solid line: results of analytical calculation in the true limit $l \to 0$. Crosses: extrapolation of the $l \neq 0$ results to $l = 0$ using the scaling $\omega(q_x, l) = \omega(q_x, l = 0) - a(q_x)l$. *Bottom*: Growth rate (left) and wavevector (right) at the peak of dispersion relations as a function of the pressure drop G, calculated analytically in the limit $l \to 0$.

basic state. These numerical results for this dispersion relation are shown by dashed lines in Fig. 3(Top), for different values of the interfacial thickness l. As can be seen, at any fixed value of q_x the growth rate shows a linear dependence on l: $\omega^*(l, q_x) = \omega^*(l = 0, q_x) - a(q_x)l$ where the intercept $\omega^*(l = 0, q_x)$ plotted versus q_x accordingly forms the dispersion relation extrapolated to $l = 0$, shown by the crosses in Fig. 3(Top). The value $l = 0$ cannot be accessed in this full nonlinear code, because this limit is pathological in shear banding fluids. However, analytical linear stability calculations can nonetheless still be performed in this limit [51]. The solid line in Fig. 3(Top) accordingly shows the results of a truly linear analytical stability calculation, performed in the true limit $l \to 0$. As can be seen, this indeed agrees well with the extrapolation of the numerical results to $l = 0$. Because the $l \neq 0$ and $l = 0$ calculations were performed independently by the two authors, and using different methods, this provides a good cross check between both sets of results.

Because of the linear nature of this calculation, any eigenvector can be separated into sinuous and varicose contributions, in which the perturbation to the flow field across the channel is odd (snake-like) and even (sausage-like) respectively. Each of these is an eigenvector in its own right. In the $l = 0$ calculations, this separation is carried out explicitly. We find that the sinuous (snake-like) modes are always more unstable than varicose ones. Because our interest is in the most unstable mode, the $l = 0$ results presented here are all for sinuous perturbations. (In our runs of the full code for $l \neq 0$, we do not impose any such symmetry a priori. Instead, it emerges naturally from the full system.)

The location of the peak in the dispersion relation is shown as a function of pressure drop G in Fig. 3(Bottom), for the $l = 0$ calculation. As can be seen, for values of G well within the banding regime the growth rate $\omega^* \approx 2$, of the same order as the linear viscoelastic relaxation time, and the wavelength $\lambda_x^* = 2\pi/q_x^* \approx 2$, comparable to twice the gap width. This is consistent with the presence of secondary velocity rolls [48,49] of a wavelength comparable to the gap width, and also consistent with the dominant wavelength seen in our nonlinear results discussed in Fig. 4. (Such velocity rolls will be shown explicitly in our corresponding study of the flow-gradient/vorticity plane in Fig. 7.) As the applied shear rate approaches the low shear branch from above, and the width of the high shear bands accordingly tends to zero, the growth rate and wavelength of the most unstable perturbations also tend to zero.

For a small range of pressure drops $1.20 < G < 1.52$, two peaks are evident in the dispersion relation (not shown). For $G \leq 1.3$ the peak with the larger value of q_x is the more unstable, with crossover to dominance of the lower q_z peak for $G \geq 1.32$. This causes a "kink" in the plot of ω^* against G at $G \approx 1.3$, only just discernible in Fig. 3, and not to be confused with the more obvious kink at $G \approx 5$.

4.2. Ultimate nonlinear dynamics

At long times the instability described above saturates at the level of finite amplitude undulations along the interface. Represen-

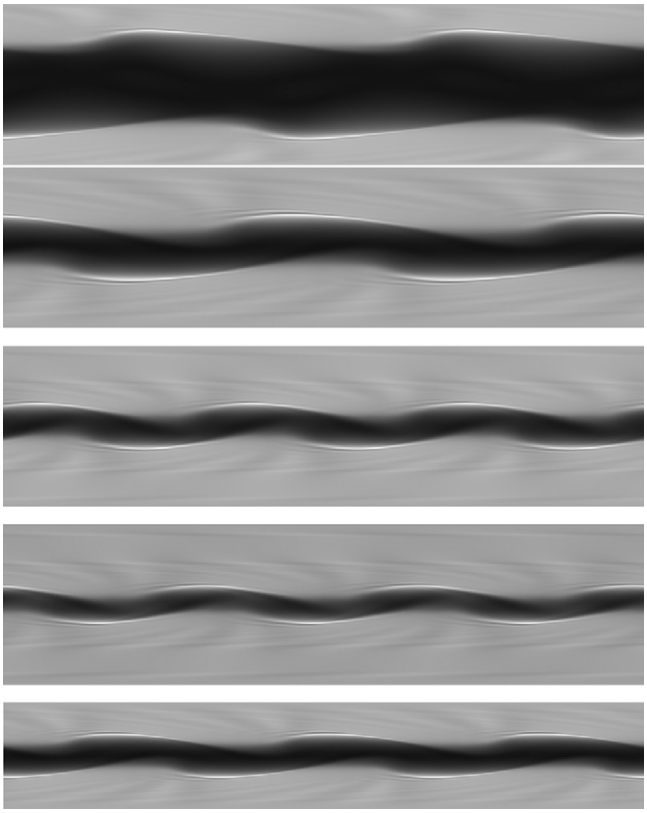

Fig. 4. Greyscale snapshots of the order parameter $\Sigma_{xx}(x, y)$ in the y (vertical) and x (horizontal) plane at a representative time $t = 60.0$ on the ultimate nonlinear attractor for $a = 0.3$, $\eta = 0.05$, $l = 0.005$ for $L_x = 4.0$ and G = 2.0, 4.0, 6.0, 8.0 (top four subfigures downwards) with $Dt = 0.000025$, $N_x = 200$, $N_y = 400$. Bottom subfigure is for $G = 4.0$ with a longer cell $L_x = 6.0$ (so $N_x = 300$).

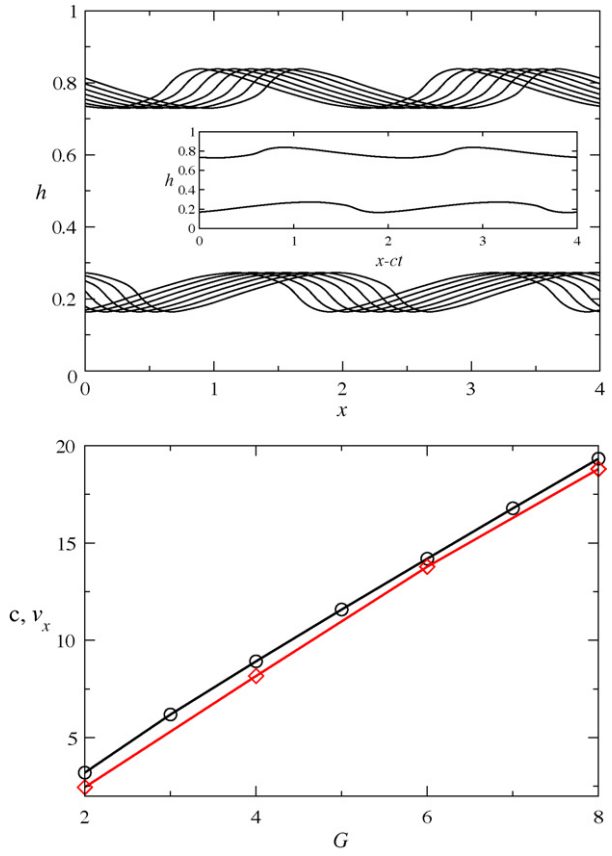

Fig. 5. *Top*: Snapshot of interface height $h(x)$ for $a = 0.3$, $\eta = 0.05$, $l = 0.005$, $L_x = 4.0$ and $G = 2.0$ at six times equally spaced by $\Delta t = 0.05265$. $Dt = 0.000025$, $N_x = 200$, $N_y = 400$. Inset: the same data plotted versus transformed coordinate $x - ct$ revealing simple convective motion with a constant wavespeed c. *Bottom*: Diamonds: wavespeed c versus pressure drop G, obtained by performing the transformation shown in Fig. 5. $a = 0.3$, $\eta = 0.05$, $l = 0.005$, $L_x = 4.0$ for runs with $Dt = 0.000025$, $N_x = 200$, $N_y = 400$. Circles: fluid velocity v_x at interface, taken from the 1D banded profiles of Fig. 2.

tative greyscale snapshots of the system's eventual state are shown in Fig. 4. As can be seen in Fig. 5(Top), the interfacial undulations convect along the positive x direction with constant speed. This is to be expected, given that fluid's main flow direction is along x. This speed is plotted as a function of pressure drop in Fig. 5(Bottom), and is comparable, but not exactly equal, to the value of the fluid velocity at the interface. As noted above, our $l \neq 0$ code does not impose any sinuous/varicose symmetry a priori.

5. Flow-gradient, vorticity plane

In this section we turn attention to the flow-gradient/vorticity (y–z) plane, now assuming translational invariance in the flow direction x. As usual we assume closed walls in y, and (for simplicity) periodic boundaries in z. We will return in the conclusion to discuss briefly the implications of having focused only on 2D studies in this paper.

5.1. Linear stability analysis

We consider first the linear stability properties of the 1D basic states of Fig. 2 with respect to fluctuations with wavevector in the vorticity direction, $\exp(iq_z z + \omega t)$. To do so we perform a truly linear calculation, calculating the eigenmodes of the stability matrix that is obtained by linearising the full nonlinear equations about the basic state. This linearisation problem was in fact studied previously in the flow-gradient/vorticity plane in the context of planar Couette flow in Ref. [52]. The same linearised code can be used here, simply inserting the new pressure driven basic state as an input to the elements of the matrix.

The resulting dispersion relations $\omega(q_z)$ are shown in Fig. 6(Top). As is evident, at each value of q_z the growth rate increases linearly with decreasing values of the interfacial width l, allowing us to extrapolate to the case $l = 0$ (thick line in Fig. 6, Top), as in the case of the x–y plane above. The location ω^*, q_z^* of the peak in the dispersion relations is plotted as a function of the pressure drop G in Fig. 6(Bottom). As can be seen, for large values of the interfacial width l the instability is absent (all $\omega^* < 0$). For intermediate values of l there is a window in G between the onset of shear banding and the onset of this interfacial instability. The size of this window decreases with decreasing l, and we believe would extrapolate to zero as $l \to 0$, such that all shear banded states are linearly unstable in the limit of a thin interface.

These truly linear results were checked for consistency against the linearised dynamics of a fully nonlinear code, which directly simulates the full 2D dynamics of the model in the yz plane. (The main use of this code is to generate the results in the next subsection.) In each run of this nonlinear code we used as an initial condition the 1D basic state of Fig. 2, subject to small 2D fluctuations in the y–z plane. By monitoring the early-time growth of

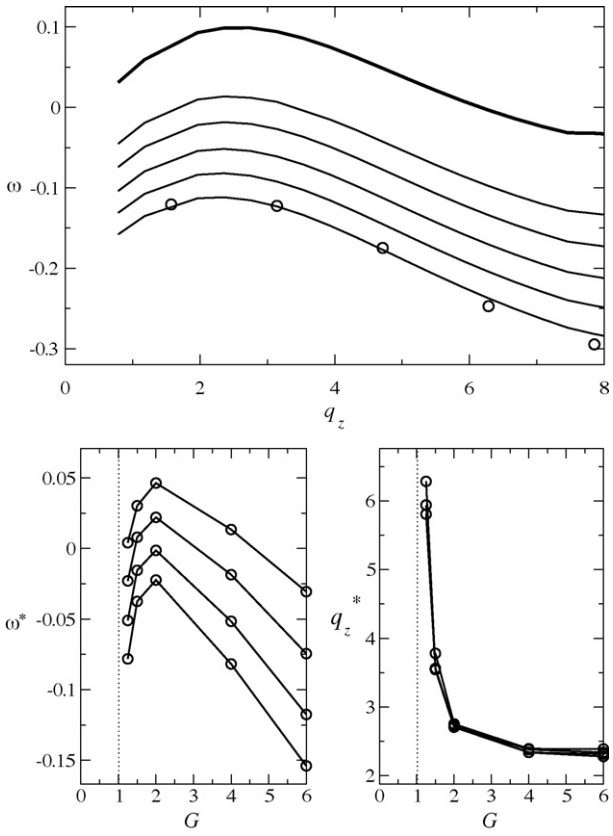

Fig. 6. *Top*: Dispersion relation of growth rate ω versus wavevector q_z during the initial stage of 2D instability, starting with a 1D shear banded planar Poiseuille basic state. In each case $a = 0.3$, $\eta = 0.05$, $G = 4.0$. Thin solid lines: calculated by linear stability analysis using the method of Ref. [52], with lines upward corresponding to $l = 0.0035$, 0.003, 0.0025, 0.002, 0.0015. Thick solid lines: extrapolation of the $l \neq 0$ results shown by each of the thin solid lines to $l = 0$ using the scaling $\omega(q_z, l) = \omega(q_z, l = 0) - a(q_z)l$. Indistinguishability of the thick lines demonstrates the validity of this scaling over the range explored here. Circles: extracted from early-time dynamics of the full nonlinear code for $l = 0.0035$. *Bottom*: Growth rate (left) and wavevector (right) at the peak of dispersion relation as a function of the pressure drop G for $l = 0.003$, 0.0025, 0.002, 0.0015 (sets upwards in left hand figure).

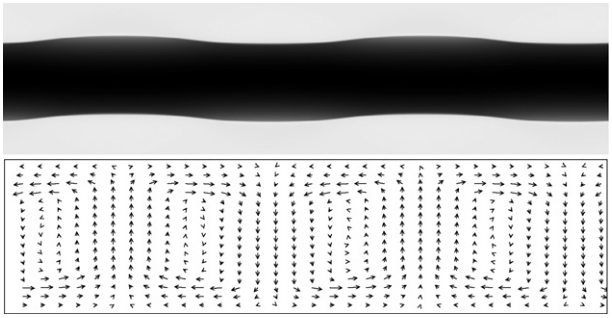

Fig. 7. Order parameter $\Sigma_{xx}(y,z)$ greyscale (top) and velocity map showing secondary flow in y (vertical) and z (horizontal) plane (bottom): snapshot at time $t = 1895$ in steady state for $a = 0.3$, $\eta = 0.05$, $l = 0.0015$ for $L_z = 4.0$ and $G = 2.0$ with $Dt = 0.05$, $N_z = 1000$, $N_y = 1066$.

the Fourier components $\exp(iq_z z)\exp(\omega t)$ we extracted the dispersion relation $\omega(q_z)$ for the linear (in)stability of the 1D basic state. As shown by the circles in Fig. 6, good agreement is found with the true linear stability calculation described in the previous paragraph. This provides a stringent cross check between our linear stability calculation and our nonlinear code.

5.2. Ultimate nonlinear attractor

In previous work we simulated the full nonlinear dynamics of the DJS model in 2D plane Couette flow in the flow-gradient/vorticity (y–z) plane [52], assuming translational invariance in the flow direction x. The code is adapted to the pressure driven flow of interest here using the simple modification already discussed above in the context of the flow/flow-gradient plane. As described in the previous section, we performed a series of runs of this code starting with a 1D basic state, subject to small 2D perturbations. In each case, the instability was found to saturate at long times in an ultimate steady state with finite amplitude undulations along the interface (Fig. 7, Top). In this plane the undulations do not convect in time. This is to be expected, because this plane is orthogonal to the main direction of flow. Such undulations have recently been imaged experimentally in the pressure driven flow of wormlike micelles in microchannels of high aspect ratio [58]. Associated with these undulations is a secondary flow comprising the velocity rolls shown in the second subfigure (Fig. 7, Bottom).

6. Summary and outlook

In this work, we have studied the pressure driven planar Poiseuille flow of a shear banding fluid sandwiched between infinite stationary flat parallel plates. Using a combination of linear stability analysis and direct numerical simulation, we have shown an initially flat interface between shear bands to be unstable with respect to the growth of undulations along it. The early-time growth rate of these undulations scales as the reciprocal stress relaxation time of the fluid, and the corresponding wavelength is comparable to the separation of the plates. At long times the undulations saturate in a finite amplitude, cutoff by the nonlinear effects of shear.

Throughout our study we have neglected any in-flow and out-flow effects at the start and end of the channel, assuming a well established flow field that is free from end effects. Associated with this is our assumption that the spatial limits relevant to this established flow field correspond to the temporal limit $t \to \infty$ in each run of our code. We have furthermore neglected the effect of any lateral walls in the z direction, taking from the outset the limit $L_z/L_y \to \infty$. In practice one might expect lateral walls to impose a further loss of translational symmetry in the z direction, as explored in Ref. [58]. Perhaps most importantly, in conducting separate two-dimensional studies in the $x-y$ and $y-z$ planes, we have neglected the possibility that exists in three spatial dimensions of nonlinear interactions between the q_x and q_z modes. Indeed, although the q_x modes have much faster growth rates than the q_z modes in the early-time (linear) growth regime, they are seen to be cut off more aggressively at nonlinear order by the effects of shear, by the fact that the q_x and q_z modes have comparable amplitudes in the ultimate attractors of our separate 2D studies. It therefore seems unlikely that 3D effects cannot be neglected, as we shall explore in future. The role of different boundary conditions [63,64] and wall slip should also be explored. We mention finally that the constitutive model used in the present work is highly oversimplified, in particular in having a Newtonian high shear branch.

Recent experiments in microchannel flow used 1D velocimetry imaging to reconstruct the local flow curves of a shear banding wormlike micellar surfactant solution [57]. Surprisingly, these curves were found to be non-universal, failing to collapse when plotted for different applied pressure gradients on a single plot. Possible explanations of this observation, to be explored in future work, include: a larger ratio l/L_y than considered here; coupling between flow and concentration; and the effects of secondary 3D flows.

Acknowledgements

SMF thanks Tony Maggs for his hospitality during a research visit, funded by the CNRS of France, to the Laboratoire de Physico-Chimie Théorique (PCT) at ESPCI in Paris, where this work was partly carried out. SMF also thanks Philippe Nghe and Patrick Tabeling in the Microfluidique, MEMS et Nanostructures group at ESPCI, and Armand Ajdari of PCT for stimulating discussions. Financial support for SMF is acknowledged from the UK's EPSRC in the form of an Advanced Research Fellowship, grant reference EP/E5336X/1.

References

[1] N.A. Spenley, M.E. Cates, T.C.B. McLeish, Nonlinear rheology of wormlike micelles, Phys. Rev. Lett. 71 (1993) 939–942.
[2] N.A. Spenley, X.F. Yuan, M.E. Cates, Nonmonotonic constitutive laws and the formation of shear-banded flows, J. Phys. II (France) 6 (1996) 551–571.
[3] J. Yerushalmi, S. Katz, R. Shinnar, Chem. Eng. Sci. 25 (1970) 1891.
[4] H. Rehage, H. Hoffmann, Viscoelastic surfactant solutions: model systems for rheological research, Mol. Phys. 74 (1991) 933.
[5] J.P. Decruppe, R. Cressely, R. Makhloufi, E. Cappelaere, Flow birefringence experiments showing a shear-banding structure in a ctab solution, Coll. Polym. Sci. 273 (4) (1995) 346–351.
[6] M.M. Britton, P.T. Callaghan, Two-phase shear band structures at uniform stress, Phys. Rev. Lett. 78 (1997) 4930–4933.
[7] P.T. Callaghan, Rheo NMR and shear banding, Rheol. Acta 47 (2008) 243–255.
[8] L. Becu, S. Manneville, A. Colin, Spatiotemporal dynamics of wormlike micelles under shear, Phys. Rev. Lett. 93 (1) (2004), art. no. 018301.
[9] S. Manneville, Recent experimental probes of shear banding, Rheol. Acta 47 (Apr 2008) 301–318.
[10] J.B. Salmon, A. Colin, S. Manneville, F. Molino, Velocity profiles in shear-banding wormlike micelles, Phys. Rev. Lett. 90 (22) (2003), art. no. 228303.
[11] Y.T. Hu, A. Lips, Kinetics and mechanism of shear banding in an entangled micellar solution, J. Rheol. 49 (2005) 1001–1027.
[12] J.F. Berret, D.C. Roux, G. Porte, Isotropic-to-nematic transition in wormlike micelles under shear, J. Phys. II (France) 4 (8) (1994) 1261–1279.
[13] P.T. Callaghan, M.E. Cates, C.J. Rofe, J.B.A.F. Smeulders, A study of the spurt effect in wormlike micelles using nuclear-magnetic-resonance microscopy, J. Phys. II (France) 6 (1996) 375–393.
[14] C. Grand, J. Arrault, M.E. Cates, Slow transients and metastability in wormlike micelle rheology, J. Phys. II (France) 7 (1997) 1071–1086.
[15] J.F. Berret, D.C. Roux, G. Porte, P. Lindner, Shear-induced isotropic-to-nematic phase-transition in equilibrium polymers, Europhys. Lett. 25 (1994) 521–526.
[16] V. Schmitt, F. Lequeux, A. Pousse, D. Roux, Flow behavior and shear-induced transition near an isotropic–nematic transition in equibrium polymers, Langmuir 10 (1994) 955–961.
[17] E. Cappelaere, J.F. Berret, J.P. Decruppe, R. Cressely, P. Lindner, Rheology, birefringence, and small-angle neutron scattering in a charged micellar system: evidence of a shear-induced phase transition, Phys. Rev. E 56 (2) (1997) 1869–1878.

[18] R. Makhloufi, J.P. Decruppe, A. Aitali, R. Cressely, Rheooptical study of worm-like micelles undergoing a shear banding flow, Europhys. Lett. 32 (3) (1995) 253–258.
[19] J.F. Berret, G. Porte, J.P. Decruppe, Inhomogeneous shear rows of worm-like micelles: a master dynamic phase diagram, Phys. Rev. E 55 (2) (1997) 1668–1676.
[20] O. Diat, D. Roux, F. Nallet, Effect of shear on a lyotropic lamellar phase, J. Phys. II (France) 3 (1993) 1427–1452.
[21] G.M.H. Wilkins, P.D. Olmsted, Vorticity banding during the lamellar-to-onion transition in a lyotropic surfactant solution in shear flow, Eur. Phys. J. E 21 (2006) 133–143.
[22] D. Bonn, J. Meunier, O. Greffier, A. Alkahwaji, H. Kellay, Bistability in non-Newtonian flow: rheology of lyotropic liquid crystals, Phys. Rev. E 58 (2 PtB) (1998) 2115–2118.
[23] J.B. Salmon, S. Manneville, A. Colin, Shear banding in a lyotropic lamellar phase. I. Time-averaged velocity profiles, Phys. Rev. E 68 (5) (2003), art. no. 051503.
[24] J.B. Salmon, S. Manneville, A. Colin, Shear banding in a lyotropic lamellar phase. II. Temporal fluctuations, Phys. Rev. E 68 (5) (2003), art. no. 051504.
[25] S. Manneville, J.B. Salmon, A. Colin, A spatio-temporal study of rheo-oscillations in a sheared lamellar phase using ultrasound, Eur. Phys. J. E 13 (2) (2004) 197–212.
[26] C. Pujolle-Robic, L. Noirez, Observation of shear-induced nematic-isotropic transition in side-chain liquid crystal polymers, Nature 409 (2001) 167–171.
[27] M.P. Lettinga, J.K.G. Dhont, Non-equilibrium phase behaviour of rod-like viruses under shear flow, J. Phys. Condens. Matter 16 (2004) S3929–S3939.
[28] J.K.G. Dhont, W.J. Briels, Inhomogeneous suspensions of rigid rods in flow, J. Chem. Phys. 118 (2003) 1466–1478.
[29] J.F. Berret, Y. Serero, Evidence of shear-induced fluid fracture in telechelic polymer networks, Phys. Rev. Lett. (2001) 8704.
[30] P. Coussot, J.S. Raynaud, F. Bertrand, P. Moucheront, J.P. Guilbaud, H.T. Huynh, S. Jarny, D. Lesueur, Coexistence of liquid and solid phases in flowing soft-glassy materials, Phys. Rev. Lett. 88 (21) (2002), art. no. 218301.
[31] W.M. Holmes, P.T. Callaghan, D. Vlassopoulos, J. Roovers, Shear banding phenomena in ultrasoft colloidal glasses, J. Rheol. 48 (Sep 2004) 1085–1102.
[32] S.A. Rogers, D. Vlassopoulos, P.T. Callaghan, Aging, yielding, and shear banding in soft colloidal glasses, Phys. Rev. Lett. 100 (Mar 2008) 128304.
[33] L. Hilliou, D. Vlassopoulos, Time-periodic structures and instabilities in shear-thickening polymer solutions, Ind. Eng. Chem. Res. 41 (25) (2002) 6246–6255.
[34] L.B. Chen, C.F. Zukoski, B.J. Ackerson, H.J.M. Hanley, G.C. Straty, J. Barker, C.J. Glinka, Structural-changes and orientational order in a sheared colloidal suspension, Phys. Rev. Lett. 69 (1992) 688–691.
[35] W.M. Holmes, M.R. Lopez-Gonzalez, P.T. Callaghan, Fluctuations in shear-banded flow seen by nmr velocimetry, Europhys. Lett. 64 (Oct 2003) 274–280.
[36] M.R. Lopez-Gonzalez, W.M. Holmes, P.T. Callaghan, P.J. Photinos, Shear banding fluctuations and nematic order in wormlike micelles, Phys. Rev. Lett. 93 (Dec 2004) 268302.
[37] R. Bandyopadhyay, G. Basappa, A.K. Sood, Observation of chaotic dynamics in dilute sheared aqueous solutions of ctat, Phys. Rev. Lett. 84 (2000) 2022–2025.
[38] R. Ganapathy, A.K. Sood, Intermittency route to rheochaos in wormlike micelles with flow-concentration coupling, Phys. Rev. Lett. 96 (2006) 108301.
[39] Y.T. Hu, P. Boltenhagen, D.J. Pine, Shear thickening in low-concentration solutions of wormlike micelles. I. Direct visualization of transient behavior and phase transitions, J. Rheol. 42 (5) (1998) 1185–1208.
[40] R. Bandyopadhyay, A.K. Sood, Chaotic dynamics in shear-thickening surfactant solutions, Europhys. Lett. 56 (2001) 447–453.
[41] E.K. Wheeler, P. Fischer, G.G. Fuller, Time-periodic flow induced structures and instabilities in a viscoelastic surfactant solution, J. Non-Newton. Fluid Mech. 75 (1998) 193–208.
[42] V. Herle, P. Fischer, E.J. Windhab, Stress driven shear bands and the effect of confinement on their structures—a rheological, flow visualization, and Rheo-SALS study, Langmuir 21 (2005) 9051–9057.
[43] P. Fischer, Time dependent flow in equimolar micellar solutions: transient behaviour of the shear stress and first normal stress difference in sheer induced structures coupled with flow instabilities, Rheol. Acta 39 (2000) 234–240.
[44] H. Azzouzi, J.P. Decruppe, S. Lerouge, O. Greffier, Temporal oscillations of the shear stress and scattered light in a shear-banding-shear-thickening micellar solution, Eur. Phys. J. E 17 (2005) 507–514.
[45] J.P. Decruppe, O. Greffier, S. Manneville, S. Lerouge, Local velocity measurements in heterogeneous and time-dependent flows of a micellar solution, Phys. Rev. E 73 (2006) 061509.
[46] J-B. Salmon, A. Colin, D. Roux, Dynamical behavior of a complex fluid near an out-of-equilibrium transition: approaching simple rheological chaos, Phys. Rev. E 66 (3) (2002), art. no. 031505.
[47] S. Lerouge, M. Argentina, J.P. Decruppe, Interface instability in shear-banding flow, Phys. Rev. Lett. 96 (2006) 088301.
[48] S. Lerouge, M.A. Fardin, M. Argentina, G. Gregoire, O. Cardoso, Interface dynamics in shear-banding flow of giant micelles, Soft Matter 4 (2008) 1808–1819.
[49] M.A. Fardin, B. Lasne, O. Cardoso, G. Gregoire, M. Argentina, J.P. Decruppe, S. Lerouge, Taylor-like vortices in shear-banding flow of giant micelles, Phys. Rev. Lett. 103 (July 2009) 028302.
[50] S.M. Fielding, Linear instability of planar shear banded flow, Phys. Rev. Lett. 95 (2005) 134501.
[51] H.J. Wilson, S.M. Fielding, Linear instability of planar shear banded flow of both diffusive and non-diffusive Johnson–Segalman fluids, J. Non-Newton. Fluid Mech. 138 (2006) 181–196.
[52] S.M. Fielding, Vorticity structuring and velocity rolls triggered by gradient shear bands, Phys. Rev. E 76 (July 2007) 016311.
[53] E.J. Hinch, O.J. Harris, J.M. Rallison, The instability mechanism for 2 elastic liquids being coextruded, J. Non-Newton. Fluid Mech. 43 (1992) 311–324.
[54] R.G. Larson, E.S.G. Shaqfeh, S.J. Muller, A purely elastic instability in taylor-couette flow, J. Fluid Mech. 218 (1990) 573–600.
[55] L. Becu, D. Anache, S. Manneville, A. Colin, Evidence for three-dimensional unstable flows in shear-banding wormlike micelles, Phys. Rev. E (2007) 76.
[56] P. Nghe, G. Degre, P. Tabeling, A. Ajdari, High shear rheology of shear banding fluids in microchannels, Appl. Phys. Lett. 93 (Nov 2008) 204102.
[57] C. Masselon, J.B. Salmon, A. Colin, Nonlocal effects in flows of wormlike micellar solutions, Phys. Rev. Lett. 100 (Jan 2008) 038301.
[58] P. Nghe, S.M. Fielding, P. Tabeling, A. Ajdari, Microchannel flow of a shear banding fluid: enhanced edge effect and interfacial instability, available at http://arxiv.org/abs/0909.1306.
[59] M.W. Johnson, D. Segalman, Model for viscoelastic fluid behavior which allows non-affine deformation, J. Non-Newton. Fluid Mech. 2 (1977) 255–270.
[60] P.D. Olmsted, O. Radulescu, C.Y.D. Lu, Johnson–Segalman model with a diffusion term in cylindrical Couette flow, J. Rheol. 44 (2000) 257–275.
[61] C.Y.D. Lu, P.D. Olmsted, R.C. Ball, Effects of nonlocal stress on the determination of shear banding flow, Phys. Rev. Lett. 84 (2000) 642–645.
[62] S.M. Fielding, Role of inertia in nonequilibrium steady states of sheared binary fluids, Phys. Rev. E 77 (2008) 021504.
[63] J.M. Adams, S.M. Fielding, P.D. Olmsted, The interplay between boundary conditions and flow geometries in shear banding: hysteresis, band configurations, and surface transitions, J. Non-Newton. Fluid Mech. 151 (May 2008) 101–118.
[64] L.P. Cook, L.R. Rossi, Slippage and migration in models of dilute wormlike micellar solutions and polymeric fluids, J. Non-Newton. Fluid Mech. 116 (January 2004) 347–369.
[65] S.M. Fielding, P.D. Olmsted, Flow phase diagrams for concentration-coupled shear banding, Eur. Phys. J. E 11 (2003) 65–83.
[66] S.M. Fielding, P.D. Olmsted, Nonlinear dynamics of an interface between shear bands, Phys. Rev. Lett. (2006) 96.